Z. Phys. Chem. **219** (2005) 1505–1518

Effect of Pretreatment on the Intermetallics in Aluminum Alloy 2024-T3

By Jana Vander Kloet, Achim Walter Hassel*, and Martin Stratmann

Max-Planck-Institut für Eisenforschung GmbH, Max-Planck-Str. 1, 40237 Düsseldorf, Germany

Dedicated to Prof. Dr. Hans-Jürgen Engell on the occasion of his 80th birthday

(Received May 15, 2005; accepted in revised form August 15, 2005)

Aluminum Alloy AA2024-T3 / Pretreatment / Filiform Corrosion / Intermetallic Particles / Scanning Kelvin Probe Force Microscopy

The effect of surface treatments on the surface characteristics of aluminium alloy 2024-T3 before the appearance of filiform corrosion (FFC) is investigated. The nature of the surface prior to coating and initiation of FFC, with particular respect to the intermetallics is investigated in this work.

The SKPFM (Scanning Kelvin Probe Force Microscopy), ToF-SIMS (Time of Flight Secondary Ion Mass Spectroscopy), XPS (X-Ray Photo Electron Spectroscopy) and SEM (Scanning Electron Microscopy) surface analysis techniques were used to characterize polished AA2024-T3 before and after etching or after etching with subsequent chromating treatments. The etching pretreatment is intended to remove surface intermetallics and increase the oxide layer thickness. In these respects, the treatment was partially successful: some, not all, of the particles were eliminated from the surface and the oxide thickness increased by about 25%. In addition, XPS depth profiling showed a copper and iron enrichment at the oxide–metal interface from this treatment.

The oxide thickness is drastically increased following the application of the chromate conversion coating. Furthermore, XPS and ToF-SIMS analysis revealed that Cu and Fe were enriched on the oxide surface indicating that either Cu is complexed into the Cr-Al layer following chromating or that the chromating coating is insufficiently formed on the Cu-containing intermetallics. SKPFM analysis provided further information on the distribution of these complexes on seen by distinct points of high potential on the treated alloy surface.

1. Introduction

This work is part of a study on the surface characteristics of aluminum alloy 2024-T3 before and after the appearance of filiform corrosion (FFC). This

* Corresponding author. E-mail: hassel@elchem.de

paper concentrates on the nature of the surface prior to coating and the initiation of FFC, while another publication [1] examined alloy samples on which corrosion has taken place.

As a light-weight alloy of increased strength, the aluminum alloy 2024-T3 is commonly used in the aircraft industry [2]. Copper, iron and magnesium additions to the alloy provide this increased strength. However, the metal inclusions also provide sites on the substrate surface where oxygen reduction can take place (this leads to aluminium dissolution) or pitting. One of the well-documented forms of corrosion which can appear under coatings on aluminium alloys is filiform corrosion [3]. This corrosion type appears as filaments underneath the coating and arises due to a differential aeration cell consisting of an anodic head and a cathodic tail [4].

Alloy surfaces are often pretreated in order to eliminate, or at least diminish the extent of corrosion. Although environmentally undesirable, one of the most common pretreatments is chromating. Surface characterization, prior to and following pretreatments, is necessary in order to further understand the role surface components play in corrosion advancement. Numerous studies have already investigated AA2024-T3 surface characteristics including AES, XPS, Raman and ToF-SIMS spectroscopies, SEM and SKPFM [5–14].

Many of these investigations have examined the interactions between chromate and intermetallic particles (IMPs). Several interesting points have come out of these works. SEM and SKPFM measurements have been used to identify differences in composition and potential of intermetallic particles on a polished, unchromated AA2024-T3 surface [10–12]. Different chromium concentrations have been identified on Cu-rich and Fe-rich particles and the aluminum matrix, with the lowest Cr concentration occurring on the Cu-rich intermetallics [5]. Dynamic and static ToF-SIMS measurements [6], as well as X-ray analysis [14] were also used to illustrate the low concentration of Cr on IMPs. AFM topographical studies also demonstrated that CCC develops much slower and results in thinner coatings on alloy intermetallics [13]. XANES spectroscopy showed that the Cr(VI)/Cr(III) ratio was much lower on intermetallic particles than on the Al matrix, suggesting that possible Cr(VI) reservoirs for ‘healing’ mechanisms are absent on these particles [6]. Raman spectroscopy results indicate that $Fe(CN)_6^{3-}$, an accelerator for CCC formation [7], may preferentially chemisorb on certain Cu-containing IMPs. This chemisorbed layer appeared to interfere with CCC development [8]. Furthermore, XPS and AES spectroscopy studies have shown that ferricyanide may complex Cr and Cu as salts present which were found in the CCC [5, 9].

These work is continued here, not only to look at chromating as a pretreatment, but also the effect of the Sanchem etching pretreatment designed to remove intermetallics prior to chromating.

Table 1. Composition (in weight percent) of aluminum alloy 2024-T3.

	Cu	Mg	Fe	Si	Zn	Ti	Cr	Other
AA2024-T3	4.35	1.50	0.50	0.50	0.25	0.15	0.10	0.20

Table 2. Contents of pre-treatment solutions.

Solution	Contents	
Sanchem 500	Phosphate cleaner with no silicate	
Sanchem 1000	Sodium bromate in nitric acid	
Alodine CCC	Chromic acid	~50–60%
	Sodium fluoride	~5–10%
	Potassium zirconate	~5–10%
	Potassium fluoroborate	~20–30%
	Potassium ferrocyanide	~10–15%

2. Experimental

The aluminum alloy samples used throughout this research were AA2024-T3. The alloy composition is given in Table 1. The AA2024-T3 samples were ground and polished to 1 μm using an ethanol-based diamond paste. These samples, along with unpolished specimens, were then treated with Sanchem 500/1000 or with Sanchem 500/1000 and Alodine 1200S solutions [15]. The Sanchem 500/1000 is an acidic phosphate solution intended to remove the intermetallic particles from the alloy surface. Alodine 1200S is a chromating solution which leads to chromate conversion coatings on aluminium surfaces. The contents of these solutions are given in Table 2. Detailed application descriptions can be found elsewhere [15].

Aluminum alloy 2024-T3 samples used for filiform investigations are listed in Table 3 along with the pre-treatments. Duplicates of each sample were also investigated and the difference in results was found to be negligible.

The techniques used in the analysis of the samples mentioned in Table 3 were Scanning Electron Microscopy (SEM), X-Ray Photoelectron Spectroscopy (XPS), Time-of-Flight Secondary Ion Mass Spectroscopy (ToF-SIMS), and Scanning Kelvin Probe Force Microscopy (SKPFM). With the exception of the optical images recorded, nearly all other measurements presented here were those determined for polished samples. The decreased surface roughness of these samples enables easier analysis with the aforementioned techniques.

Table 3. Samples used in the investigation of AA2024-T3.

Sample	Polished	Sanchem	Alodine
1			
2		×	
3		×	×
4	×		
5	×	×	
6	×	×	×

SEM (CamScan 4, Elektronenoptik, Germany) provided detailed images of the surface morphology and, through Energy Dispersive X-Ray (EDX) analysis, chemical compositions of intermetallic particles and the aluminum matrix. Depth profiles were obtained with XPS (Quantum 2000, PHI, USA). The source used was monochromated Al. The sputter rate used was 2.5 nm/min (based on SiO_2). ToF-SIMS (Trift II, PHI, USA) was used to determine element distributions on the sample surfaces. The primary ion source was a gallium gun operated at 25 kV. All samples were pre-sputtered to remove atmospheric depositions and the image acquisition time was 6 min. Sample topography and surface potential differences were recorded using SKPFM (Dimension 3100, Digital Instruments, Veeco, USA).

3. Results

In the following sections, the results and discussion will be focused on samples 4–6. Although all of the aforementioned analyses were also performed for unpolished samples (1–3), the rough surface topography created measurement difficulties, especially for SKPFM.

3.1 SEM

The surface morphology of samples 4–6 can be seen in Figs. 1–3. In Fig. 1, at least two types of intermetallics, those with or without well defined edges, can be seen. Upon comparison of these intermetallics with the EDX analysis given in Table 4, it is obvious that those intermetallics with sharp edges and corners correspond to Cu-Mn-Fe particles (spots 1, 2, 4, 6) while more rounded particles contained Cu-Mg (spots 3, 5, 7). This is in agreement with previous work [10, 11]. Also seen in Fig. 1 are holes in the surface where intermetallics have fallen away from the bulk aluminum.

Once the alloy surface has been etched using the Sanchem solutions, the number of surface holes increases, indicating that a large number of the bigger particles have been removed through this treatment process (see Fig. 2).

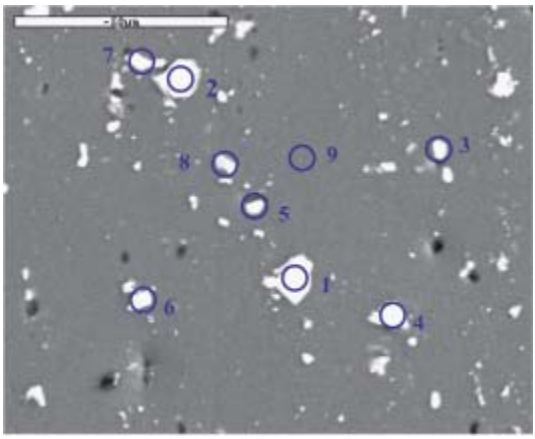

Fig. 1. SEM surface image of sample 4 (Polished).

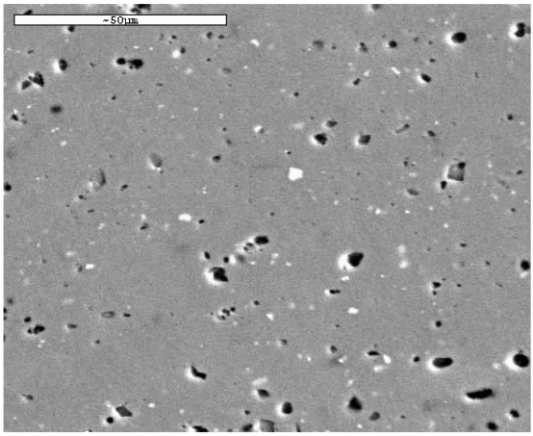

Fig. 2. SEM surface image of sample 5 (Polished, Sanchem).

However, the Sanchem process is not completely effective as numerous small intermetallics are still visible in Fig. 2. Following the Alodine pretreatment, the smaller intermetallics were still observable (Fig. 3) and the macroscopic surface morphology remained unchanged.

Tables 5 and 6 provide chemical information on various spots from samples 5 and 6, respectively (images corresponding to these spots are not provided). In general, EDX analysis was more difficult on samples 5 and 6 particles because of their small size. This typically led to unusual compositional results since the scan area ($6 \times 6\,\mu m$) often included the matrix surrounding a particular particle. For example, spots 6–8 in Table 5 illustrate this point clearly where

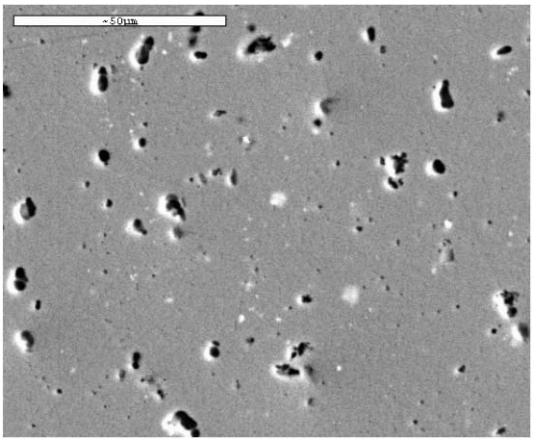

Fig. 3. SEM surface image of sample 6 (Polished, Sanchem, Alodine).

Table 4. EDX analysis of spots labelled in Fig. 1.

Spot	Cr	Al	Cu	Mn	Mg	Fe
1	0	75.8	11.0	4.1	0	9.2
2	0	75.4	17.8	1.3	0	5.5
3	0	76.5	12.5	0	11.0	0
4	0	76.5	11.9	3.6	0	8.0
5	0	79.2	10.8	0	10.0	0
6	0	85.6	10.1	1.1	0	3.2
7	0	75.6	13.4	0	11.1	0
8	0	86.8	7.3	0	5.9	0
9	0	97.0	1.6	*	1.2	0

* traces less than 0.5%

most likely small Cu-Mn-Fe particles and the aluminum matrix (often contains a few percent of Mg, Cu, Mn) were included in the analysis areas.

The traces of Fe found in the majority of spots and matrix analyses on sample 6 (Table 6) will be explained in the following section.

3.2 XPS and ToF-SIMS

The XPS sputter profiles of samples 4–6 (Fig. 4a, b, c) revealed several interesting surface characteristics. Fig. 4a demonstrates that the major surface component contains oxide which gradually decreases with depth until the substrate is reached at which point elemental aluminum and copper are easily recognizable. The iron alloy component was undetectable on this sample. The

Table 5. EDX analysis of various spots on samples 5.

Spot	Cr	Al	Cu	Mn	Mg	Fe
1	0	90.7	8.1	*	1.0	0
2	0	77.7	21.8	*	0	*
3	0	75.7	12.7	0	11.6	0
4	0	79.8	10.4	0	9.7	0
5	0	85.6	13.2	*	1.0	0
6	0	92.2	5.0	0.5	1.1	1.2
7	0	89.0	7.4	0.6	0.9	2.1
8	0	88.4	7.6	0.9	0.8	2.3
Matrix	0	96.7	1.9	*	1.2	0
Matrix	0	96.7	1.7	*	1.3	0

* traces less than 0.5%

Table 6. EDX analysis of various spots on sample 6.

Spot	Cr	Al	Cu	Mn	Mg	Fe
1	1.1	76.6	11.7	0	10.4	*
2	1.3	66.0	16.8	0	15.8	*
3	4.9	76.6	1.9	*	0	14.3
4	2.6	78.7	18.4	0	0	*
5	1.6	90.4	7.6	*	0	*
6	1.7	89.1	8.7	*	0	*
7	1.4	62.9	35.7	0	0	0
8	1.4	75.3	23.1	0	0	*
Matrix	1.3	95.4	1.8	*	1.0	*
Matrix	1.1	95.8	1.8	*	1.1	0
Matrix	1.3	96.5	1.9	*	0	*
Matrix	1.4	96.4	2.0	*	0	0

* traces less than 0.5%

oxide layer was approx. 30 nm based on the 2.5 nm/min sputter rate which is in agreement with AES depth profiles for polished AA2024-T3 [5].

Following a Sanchem surface treatment, the depth profile changes significantly (Fig. 4b). While the oxide and aluminium curves remain nearly identical to those of Fig. 4a, the copper and iron profiles show an enrichment of both elements at the oxide–metal interface. This enrichment has also been seen in recent XPS/TEM studies of AA2024-T3 samples which were submitted to an acidic etching solution [16]. The oxide layer on sample 5 was approx. 38 nm, about a 25% increase in thickness from the oxide layer on sample 4.

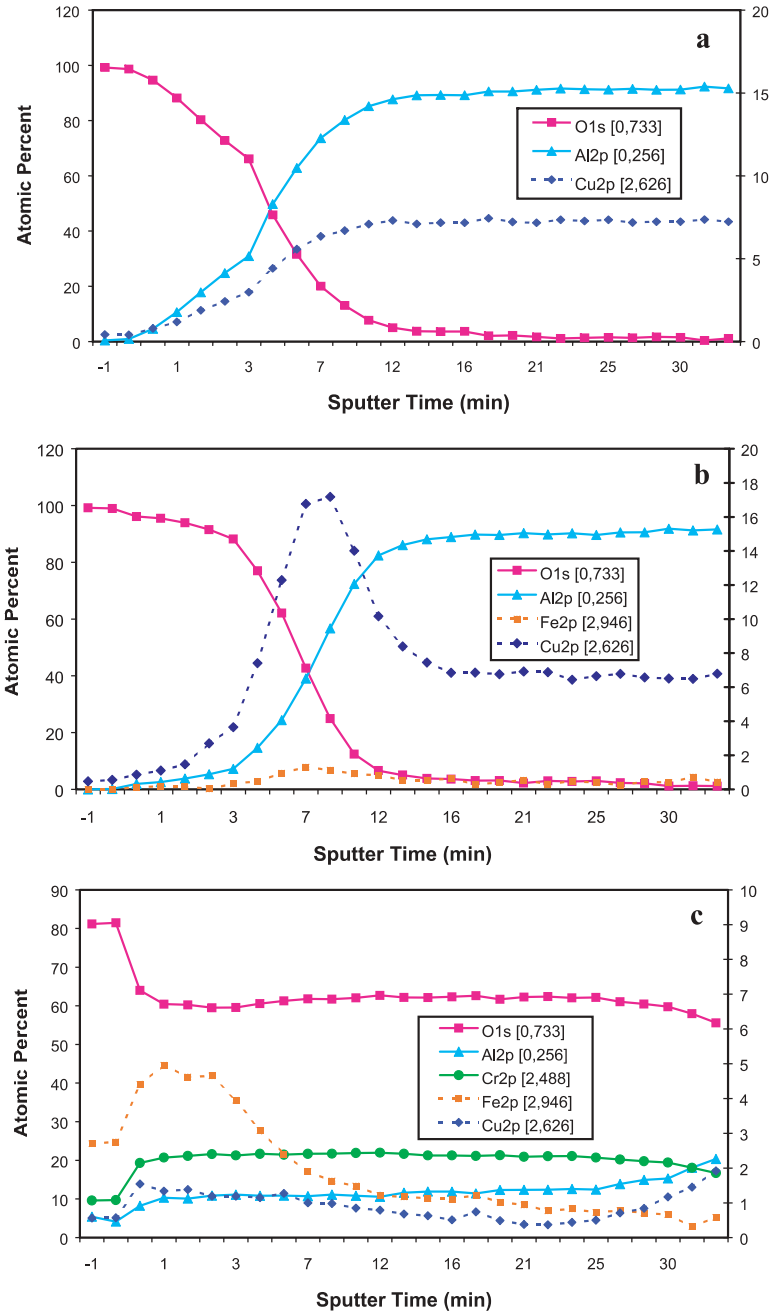

Fig. 4. XPS depth profiles of a) Sample 4, b) Sample 4 and c) Sample 6 (dotted lines refer to curves plotted with the secondary *y* axis).

Fig. 4c shows the influence of chromating on the oxide composition. The slight increases/decreases at low sputter times in the curves of Fig. 4c indicate the removal of atmospheric depositions from the surface. Upon examination of this graph, iron and copper were both enriched at the oxide surface. Iron surface enrichments explain the Fe traces found in EDX matrix analysis of sample 6 (see Table 6). Aluminum and chromium concentrations remained relatively constant throughout the oxide, indicating the little chemical change of the mixed oxide with respect to these elements. The oxide thickness also increased drastically (> 80 nm) following chromating. Oxide thicknesses of 77–84 nm and 85 nm have previously been reported for AA2024-T3 samples exposed to a similar chromating solution as that used in this work [5, 16].

ToF-SIMS analysis provides chemical information on only the outmost layer of the oxide surface, but is more sensitive than XPS to minute quantities of surface components. However, quantification of ToF-SIMS results for comparison purposes is not advisable since the amount of secondary ions which are released is strongly dependent on the matrix composition [17]. ToF-SIMS analysis was instead used as a sensitive detection technique for identifying chemical trends and relationships. Fig. 5 shows a comparison between the XPS and ToF-SIMS results for the first 0.2 nm of all three surfaces. Both analyses reveal the same trends for samples 4–6, including the iron and copper enrichment at the oxide surface following chromating (Fig. 5c).

3.3 SKPFM

The topographical and potential mapping of samples 4–6 is provided in Figs. 6–8. The potential distribution image for the polished AA2024-T3 sample (Fig. 6) illustrates that alloy intermetallics have a higher potential compared to the bulk substrate. Potential differences between the intermetallics were also observed in this work. Guillaumin *et al.* [12] reported that those intermetallics of lower potential were found to correspond to Al-Cu-Mg particles and those of higher potential to Al-Cu-(Fe,Mn) particles. Furthermore, the particles found in Fig. 6b do not necessarily correspond to topographical features of Fig. 6a.

As mentioned previously, the Sanchem solutions were not entirely effective in removing all surface particles. This result was confirmed by the potential map of sample 5 (Fig. 7b) which shows several spots of high potential. These spots are significantly smaller than those found on the untreated polished sample and the potential difference is also diminished. In addition, most of the high potential spots correspond to surface holes identified in the topography image (Fig. 7a) which also suggests that remnants of large particles were still present following the Sanchem treatment.

The Alodine chromating process led to an increased surface roughness (see Fig. 8a) from 300 to 600 nm height difference. Surface roughness factors were

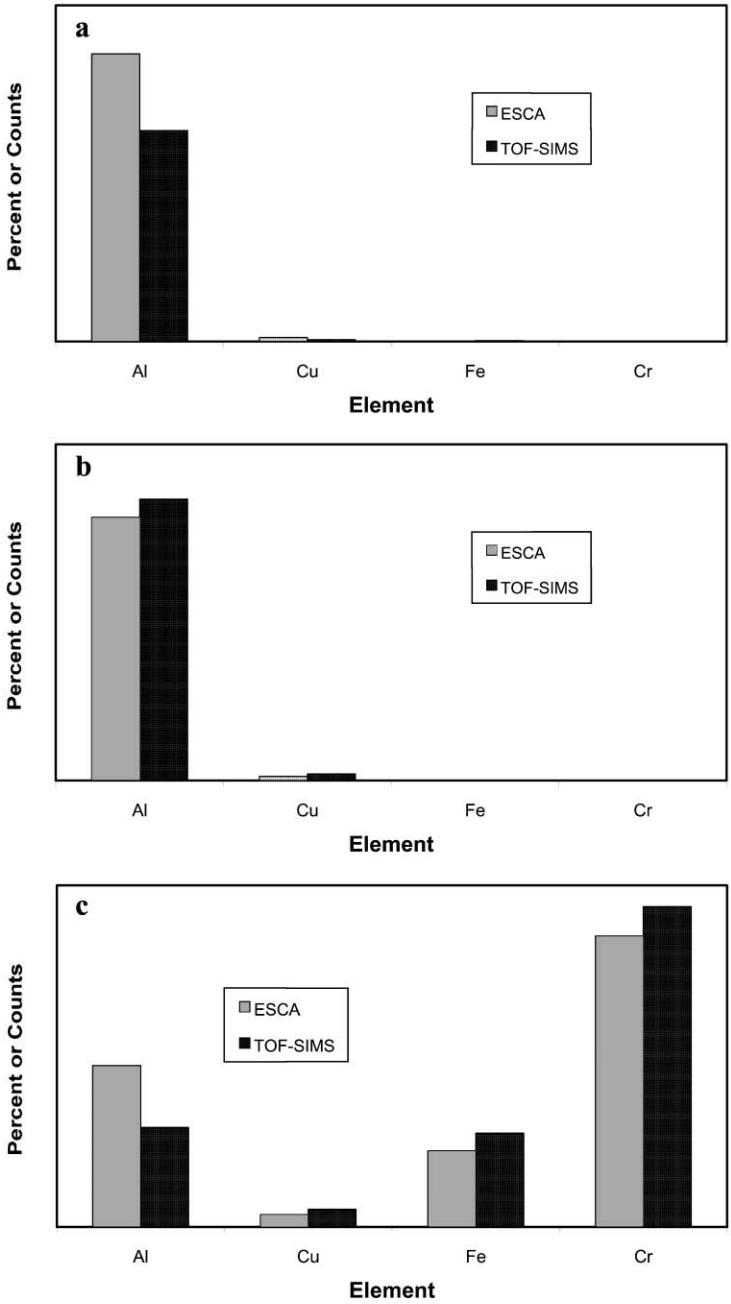

Fig. 5. Trend comparison between XPS and ToF-SIMS surface analysis of the first 0.2 nm for a) Sample 4, b) Sample 5 and c) Sample 6.

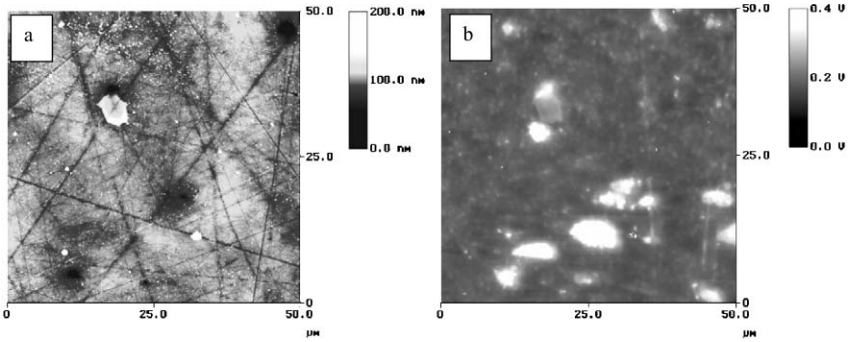

Fig. 6. SKPFM analysis of sample 4, a) topography, b) surface potential.

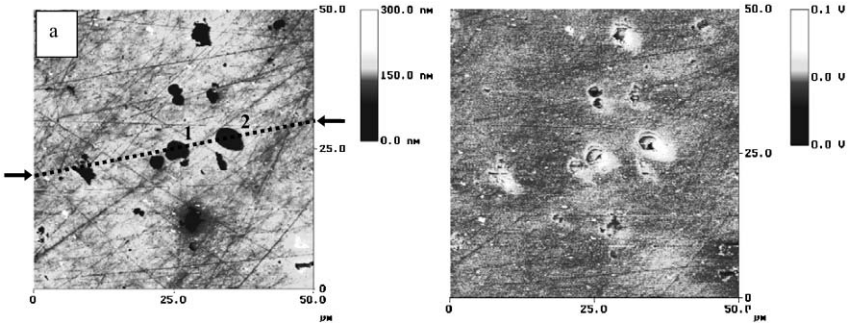

Fig. 7. SKPFM analysis of sample 5, a) topography, b) surface potential (black line marks cross-section shown in Fig. 9a).

calculated for Figs. 6a, 7a and 8a using a $12 \times 12\,\mu m$ box area. Surface holes or protrusions were purposely excluded from these measurements. The results given in Table 7 are averages of at least three measurements. It is clear from these data that surface roughness increased by a factor of 2 with the Sanchem process and by a factor of 4 following the Sanchem plus chromating pretreatments.

Sample	4	5	6
Roughness factor (rms)	6.0	10.0	22.9

Recent investigations [18] using confocal laser scanning microscopy (CLSM) have also illustrated a higher degree of surface roughness on chromated samples along with cracks and pores in the CCC. However, the depth of these cracks or holes was undeterminable with CLSM.

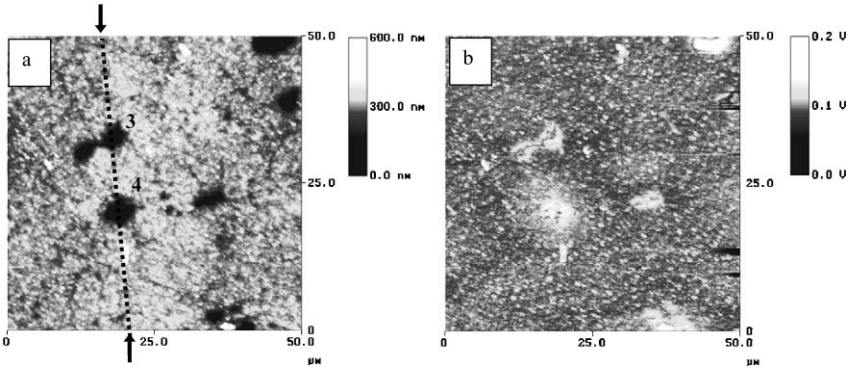

Fig. 8. SKPFM analysis of sample 6, a) topography, b) surface potential (black line marks cross-section shown in Fig. 9b).

Table 7. Depth and width of holes in Figs. 7a and 8a.

Hole	1	2	3	4
Depth (nm)	220	650	560	920
Width (μm)	4.3	5.0	4.5	5.5

Sample cross-sections of the sample surface were taken from Figs. 7a and 8a are shown in Figs. 9a and 9b, respectively. From the hole depth and width measurements given in Table 7, it is immediately obvious that the hole depth in sample 6 (holes 3 & 4) has greatly increased. This suggests that the chromate coating is insufficiently formed over the intermetallics traces found at said holes. This is in agreement with previous studies which have shown that thinner conversion coatings form on intermetallics [5, 6, 13].

Chromating also led to spots of high potential as seen in the surface potential image (Fig. 8b). These high potential spots were evenly distributed over the matrix surface, but appear to be more concentrated at locations corresponding to certain intermetallic remnants. As with the Sanchem pretreated samples, remnants of intermetallics maintained a high surface potential following chromating. Given the XPS results of the previous section and previous studies [5], these spots may be an Fe- or Cu-enriched layer introduced during the chromating process. The fact that the Fe- or Cu-containing spots of high potential appear to be concentrated at certain intermetallics supports the previous work [8] which showed preferential chemisorption of $Fe(CN)_6^{3-}$ on copper particles. The presence of either metal at the surface may explain why FFC is not completely eliminated from chromated AA2024-T3 samples.

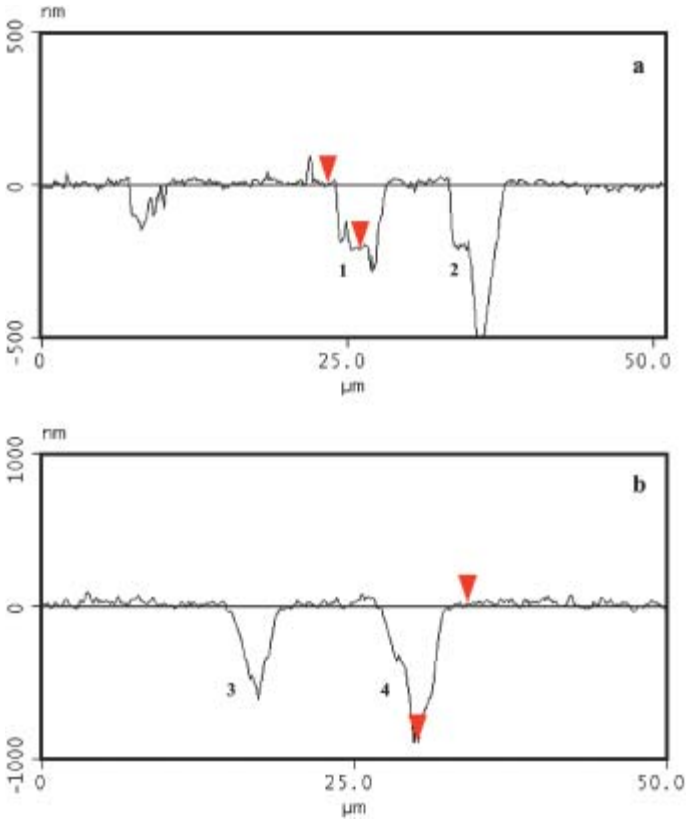

Fig. 9. Cross-section profiles from a) Fig. 7a and b) Fig. 8a (numbers correspond to holes labelled in Figs. 7a and 8a).

4. Conclusion

In this work, the effects of Sanchem and Alodine chromating pretreatments on the surface characteristics of polished AA2024-T3 were investigated. It was shown that the Sanchem pretreatment increases the Al oxide layer, but is not completely effective at removing all surface intermetallics. Furthermore, copper and iron were found in an enrichment at the oxide–metal interface.

Chromating drastically increased oxide thickness and led to a Cu and Fe enrichment at the oxide surface which was also evident as distinct points of high potential in SKPFM analysis. This suggests that either Cu is complexed into the Cr-Al layer following chromating or that the chromating coating is insufficiently formed on the Cu-containing intermetallics. This enabled the chemisorbed $Fe(CN)_6^{3-}$ layer on the Cu particles to be seen with XPS and ToF-SIMS.

Acknowledgement

The authors wish to acknowledge G. Frankel (Ohio State University) for his organization and coordination of the MURI project of which this work is a part. Special thanks are extended to R. Granata of Florida Atlantic University (Seatech) for sample preparation.

References

1. J. Vander Kloet, A. W. Hassel, and M. Stratmann, Electrochim. Acta **48** (2003) 1211.
2. T. Lyman and W. Schmidt (Eds.), *Metals Handbook*, 8th edn., Vol. 1, American Society for Metals, Ohio (1961).
3. A. Bautista, Prog. Org. Coat. **28** (1996) 49.
4. R. T. Ruggeri and T. R. Beck, Corrosion-Nace **39** (1983) 452.
5. P. L. Hagans and C. M. Haas, Surf. Interf. Anal. **21** (1994) 65.
6. G. P. Halada, C. R. Clayton, M. J. Vasquez, and J. R. Kearns, Proc. Electrochem. Soc. **98** (1999) 139.
7. L. Xia and R. L. McCreery, J. Electrochem. Soc. **146** (1999) 3696.
8. W. R. McGovern, P. Schmutz, R. G. Buchheit, and R. L. McCreery, J. Electrochem. Soc. **147** (2000) 4494.
9. A. E. Hughes, R. J. Taylor, and B. W. R. Hinton, Surf. Interf. Anal. **25** (1997) 223.
10. P. Schmutz and G. S. Frankel, J. Electrochem. Soc. **145** (1998) 2285.
11. P. Schmutz and G. S. Frankel, J. Electrochem. Soc. **145** (1998) 2295.
12. V. Guillaumin, P. Schmutz, and G. S. Frankel, J. Electrochem. Soc. B **148** (2001) 163.
13. J. R. Waldrop and M. W. Kendig, J. Electrochem. Soc. **145** (1998) L11.
14. L. Juffs, A. E. Hughes, and P. J. K. Paterson, Micron **32** (2001) 777.
15. R. R. Miron, M. M. Madani, and R. D. Granata, Specimen Preparation: CCC and Polymer Coating of Al Substrates, in *Mechanism of Al Alloy Corrosion and the Role of Chromate Inhibitors*, 2nd Ann. Rep., AFOSR Multidisciplinary University Research Initiative, Contract No. F49620-96-1-0479 (1998).
16. X. Sun, R. Li, K. C. Wong, and K. A. R. Mitchell, J. Mater. Sci. **36** (2001) 3215.
17. J. C. Newman, B. A. Carlson, R. S. Michael, and J. F. Moulder, *Static SIMS Handbook of Polymer Analysis*, T. A. Hohlt (Ed.), Perkin-Elmer Corporation, Physical Electronics Division, Eden Prairie, MN (1991).
18. G. O. Ilevbare and J. R. Scully, J. Electrochem. Soc. B **148** (2001) 196.